Article

Evolution of Coal Petrophysical Properties under Microwave Irradiation Stimulation for Different Water Saturation Conditions

He Li, Baiquan Lin, Zhongwei Chen, Yi-du Hong, and Chunshan Zheng

Energy Fuels, **Just Accepted Manuscript** • DOI: 10.1021/acs.energyfuels.7b00553 • Publication Date (Web): 02 Aug 2017

Evolution of Coal Petrophysical Properties under Microwave Irradiation Stimulation for Different Water Saturation Conditions

He Li,[a,b] Baiquan Lin,[*,a] Zhongwei Chen,[b] Yidu Hong,[a] and Chunshan Zheng[b]

[a] School of Safety Engineering, State Key Laboratory of Coal Resources and Safe Mining, China University of Mining and Technology, Xuzhou, Jiangsu 221116, China

[b] School of Mechanical and Mining Engineering, The University of Queensland, St Lucia, QLD 4072, Australia

ABSTRACT: Coalbed methane (CBM) reservoirs generally have very low permeability and requires stimulation to make gas extraction economical. Hydraulic fracturing has been widely applied to enhance CBM productivity, but this technology has a number of key limitations, including fractures only propagate along existing joints, large amount of water usage, and potential environmental impact. Microwave irradiation technology can likely overcome the above limitations. In this study, the effect of microwave irradiation on the petrophysical properties of an unconstrained bituminous coal was comprehensively investigated through a suite of integrated diagnostic techniques including Nuclear Magnetic Resonance and X-ray Computed Tomography. A series of experiments were conducted both on centrifuged samples and on samples with different water contents ranging from 1 to 15%. The mineral removal and moisture evaporation due to the microwave selective heating lead to the enlargement, opening, and interconnection of coal pores. The NMR-determined porosity increases linearly with the microwave power while grows exponentially with respect to water contents. When the water content is above 6%, the porosity increases by around 98~211%. The fracture volume and coal permeability increase while the P-wave velocity decreases with increasing water contents. Microwave irradiation is effective in enlarging mesopores and macropores and in enhancing the pore connectivity. The significant enhancement of coal permeability and pore fracture structure indicates that the microwave irradiation is effective in improving gas productivity thus has the potential to become a new CBM reservoir simulation technology.

KEYWORDS: Reservoir stimulation; Microwave irradiation; Nuclear Magnetic Resonance; Coal permeability; Water content

1. INTRODUCTION

Coalbed methane (CBM) is a safety hazard as well as an energy resource to coal mining industry.[1, 2] On the one hand, it permeates most coalbeds, rendering a danger of gas explosion and outbursts.[3, 4] Also, methane's "greenhouse gas" potential is much greater than CO_2, so its release during coal mining and processing is a concern.[5, 6] Furthermore, the release of CBM in the openings can significantly increase the ventilation expense. On the other hand, CBM can be used to generate electricity, either at mine sites or can be piped to commercial utilities.[7, 8] Therefore, CBM recovery before coal extraction is desirable.[9]

Coal has a dual-porosity system: cleats are the main gas flow path and matrices are the main location for CBM storage.[9, 10] Coal matrices generally have low permeability, and gas flow is primarily through diffusion from matrix surface to cleats. To make CBM extraction economical, it often requires an extra stimulation process. Many stimulation methods have been developed, such as hydro-fracturing, -flushing, and -slotting, CO_2-ECBM, electrochemical modification, and super-cooling etc.[10-14] However, these methods meet associated environmental and economic challenges. After invading into the coalbed, the water cannot be completely discharged because of the capillary pressure.[15, 16] As a result, the desorption, diffusion, and permeation of gas in the pores and fractures are hindered.[17] Therefore, alternative stimulation approaches are desirable to remove the water for CBM production.

Microwave lies between the far-infrared wave and the ultra-short wave within the space electromagnetic spectrum, corresponding to frequencies from 0.3 to 300 GHz.[18] In recent a few decades, microwave irradiation has gained widespread popularity in industrial, scientific, and medical applications for processing, drying, and heating.[19-22] Microwave heating has been applied for improved coal grindability, rapid coal coking, and enhanced coal cleaning.[23-27] In conventional heating, heat penetrates materials from outside inwards, while microwaves heat materials volumetrically, thus minimizing heat loss and improving efficiency.[28, 29] Another advantage of microwave heating is that it can selectively heat certain phases in a mixture more rapidly than others.[30] The microwave-material interaction depends on the dielectric property of the material.[31] Polar molecules (e.g. moisture and pyrite) have higher dielectric permittivities compared to the organic matter in the coal.[32, 33] Therefore, when coal is microwave treated, localized, and rapid superheating occurs,[34] which might affect the petrophysical properties of coal.

Liu et al.[35] presented the pore structure and fractal analysis of Ximeng lignite before and after microwave irradiation without external stress. The results showed that as the microwave power level and irradiation time increase, the specific surface area of coal decreases, whereas the pore diameter and pore

volume increase. Kumar et al.[36] used high-energy microwaves to irradiate an isotopically stressed and an unstressed bituminous coal core. They found that after microwave treatment, the aperture of the existing fractures increases and, at the same time, new fractures are created. However, few studies have investigated the effects of microwave power and water content (which contributes greatly to the dielectric property) on the petrophysical properties of coal, such as porosity, fracture network, and permeability. This aspect is critical in optimizing the implementation of this stimulation method.

In this work, an experimental investigation is conducted to study the effect of microwave irradiation on the petrophysical properties of coal under different saturation conditions. A suite of integrated diagnostic techniques including Nuclear Magnetic Resonance (NMR) and X-ray Computed Tomography (X-ray CT) are employed to monitor the dynamic response of coal properties to microwave irradiation stimulation. After that, the pore structure, porosity, and permeability of centrifuged and water-saturated coals before and after microwave irradiation are evaluated in detail. In the end, the effects of microwave power and water content on microwave fracturing and pore modification are discussed.

2. MECHANISM OF MICROWAVE HEATING

Microwaves are not heat, but rather, are energy that manifest as heat through the interaction with materials.[21] Electromagnetic heating is realized by ionic conduction, electronic, atomic, dipole, and Maxwell–Wagner polarization mechanisms.[29] At microwave frequencies, dipole polarization is regarded as the most important mechanism for energy transfer.[28] When polar molecules containing dipoles are exposed to microwave irradiation, the dipoles will attempt to align with the electromagnetic field.[32] Since the electromagnetic field is oscillating, the dipoles have to realign constantly to follow this movement (Figure 1). This continual reorientation of the molecules results in friction and consequently heat loss.

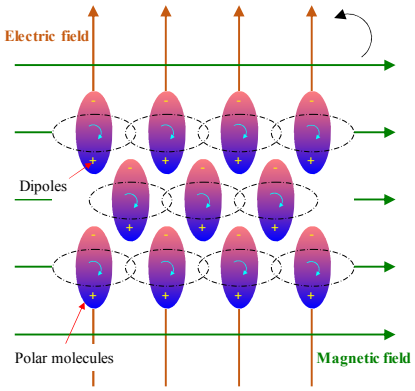

Figure 1. Realignment of polar molecules in an electromagnetic field (modified by Marland et al.[23]).

In general, microwaves are either transmitted, reflected or absorbed by a material depending on the

dielectric property (Figure 2). The dielectric property of a material is subsumed in the complex permittivity ε in the form:[33]

$$\varepsilon = \varepsilon' - j\varepsilon'' \quad (1)$$

where the real part ε' reflects the capacity of the material to store electromagnetic energy, and the imaginary part ε'' represents the dissipation of the stored energy into heat.

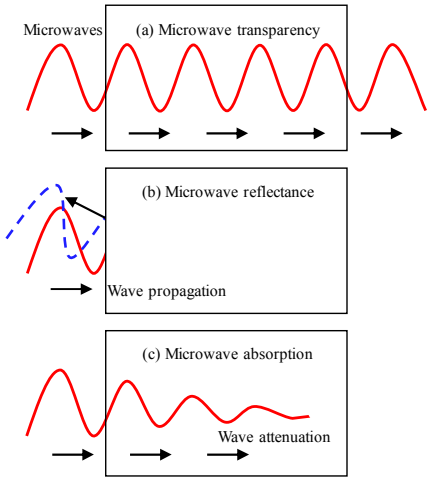

Figure 2. Behavior of a material within a microwave field.

When irradiating a material with heterogeneous dielectric properties, microwaves can selectively heat the adsorbing phase while passing through the transparent phase.[37] It is demonstrated that the organic components of coal presents low dielectric permittivity, and is essentially transparent to microwaves. On the contrary, the polar molecules (i.e. moisture and some minerals including pyrite) have higher permittivity (e.g. the ε'' of water reaches 78.54 at 25℃) and can be heated by the microwave.[38]

3. EXPERIMENTAL METHODS

3.1. Sample Preparation and Characterization.

The coal samples for this investigation were collected from the Shenmu Coalfield, China. Each lump-sized coal was drilled along the bedding direction, and then divided into two parts: cylinder cores (50 mm in diameter and 60 mm in length) and cuttings. Thirty cores were prepared for microwave irradiation, and the cuttings were used to analyze the raw coal properties (as listed in Table 1).

Table 1. Raw Coal Properties.

Coal rank	$R_{o,max}$	Proximate analysis (wt, %)				Coal maceral composition (%)				ϕ_T	ϕ_P	k_N	P_v
	(%)	M_{ad}	A_d	V_{daf}	FC_{ad}	V	I	L	M	(%)	(%)	(mD)	(km/s)

Bituminous	1.45	2.56	12.10	32.75	52.59	65.89	31.51	—	2.60	0.48	0.13	0.046	1.93

Notes: M_{ad}, moisture, air-drying basis; A_{ad}, ash yield, air-drying basis; V_{daf}, volatile matter dry ash-free basis; FC_{ad}, fixed carbon content, air-drying basis. V, Vitrinite; I, Inertinite; L, Liptinite; M, Mineral; ϕ_T, NMR-determined total porosity; ϕ_P, NMR-determined producible porosity; k_N, NMR-determined permeability; P_v, P-wave velocity.

3.2. Experimental Procedure.

The experimental procedure is illustrated in Figure 3 where the green arrows designate the experiment sequence and the red arrows indicate the measurement sequence. In a single experiment, the centrifuged coal was first saturated to reach a certain water content and then microwave irradiated for 30 seconds at different power levels. The water content (C, %) of each sample was achieved by using a gravimetric method:

$$C = \frac{W_2 - W_1}{W_1} \times 100\% \quad (2)$$

where W_1 is the initial weight of the centrifuged coal, and W_2 is the final weight of the saturated coal.

The NMR signals, X-ray CT images, and P-wave velocities of the samples were captured before and after microwave irradiation to evaluate the effect of microwave on the evolution of coal petrophysical properties. These measurements are nondestructive to the samples. Prior to NMR measurement, the sample was vacuumed for 8 hours and then saturated in distilled water for another 8 hours to reach a fully water-saturated condition (S_w). The NMR T_2 spectrum of the sample was first measured at S_w. After that, the same sample was centrifuged until reaching an irreducible water condition (S_{ir}) and the T_2 spectrum measurement was repeated (the centrifuging pressure and time are 1.4 MPa and 1.5 h, respectively).

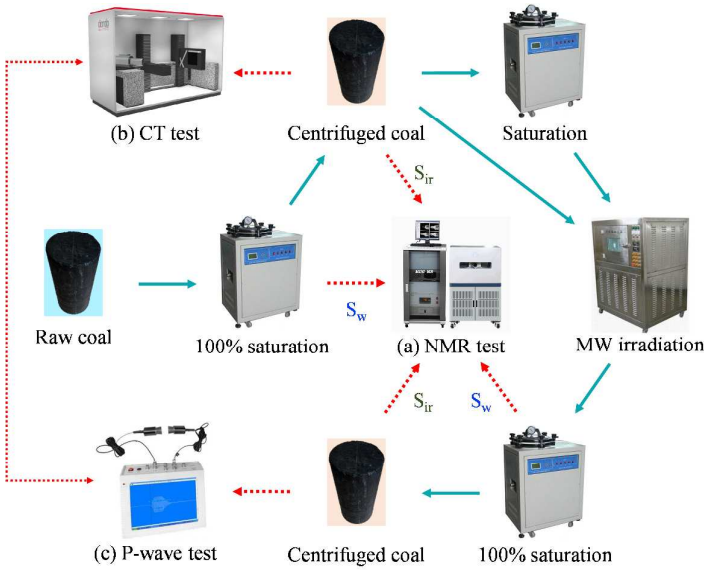

Figure 3. Experimental procedure and the corresponding apparatuses.

3.3. Microwave Irradiation System.

Microwave irradiation was performed via a microwave reaction workstation (WLD10S; Nanjing Sanle Microwave Technology Development Co., LTD, China) with adjustable powers at 2.45 GHz, as shown in Figure 4. The workstation consists of a microwave generator, a waveguide, a multimode cavity, and a console. The microwave generator has five power settings (i.e., 2 kW, 4 kW, 6 kW, 8 kW, and 10 kW). During the experiments, high-purity nitrogen (99.99%) was pumped in the cavity at a velocity of 1 L/min to create an inert atmosphere as well as release the generated vapors.

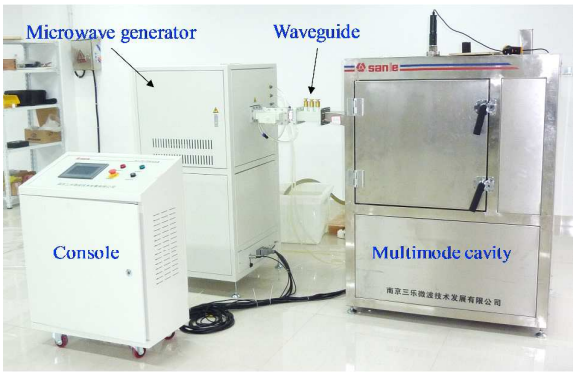

Figure 4. Microwave irradiation system.

3.4. NMR Measurements.

In the magnetic field, the hydrogen atoms present within the fluid can be detected by the transversal relaxation time (T_2), thus the pore properties can be analyzed.[39-41] T_2 can be expressed as:[42]

$$\frac{1}{T_2} = \rho \times \frac{S}{V} = \frac{a}{r} \quad (3)$$

where ρ is a constant representing the transverse relaxation strength, S is the pore surface, V is the pore volume, r is the pore radius, and a is a pore shape factor.

It can be seen from eq (3) that larger pores have longer T_2, and the higher the T_2 spectrum, the more the pores. In addition, continuity between T_2 spectrum peaks represents the pore connectivity.[43, 44] For coals, T_2<10 ms corresponds to micropores, 10 ms<T_2<10~100 ms corresponds to mesopores, and T_2>100 ms corresponds to macropores.[45] The NMR measurements were conducted using a Meso MR23-060H-I NMR spectrometer manufactured by Suzhou Niumag Analytical Instrument Corporation (see Figure 3a). After each measurement, the T_2 spectrum was computed by the simultaneous iterative reconstruction with one million iterations.

The NMR-determined total porosity (ϕ_T) is defined as the pore volume fraction occupied by bound and free water. It includes the producible porosity (ϕ_P) corresponding to connective pores and the irreducible porosity (ϕ_I) corresponding to closed pores.[46] The producible porosity contributes greatly to gas

permeability, and thus is an important parameter for evaluating CBM reservoir.

To calculate the porosity, a $CuSO_4$ solution was prepared to establish the standard equation (the relationship between the porosity and the fluid volume):[47]

$$\phi_T = \frac{V'}{V} \times 100\% = \frac{6S + 9250}{10000V} \times 100\% \quad (4)$$

where V' and V are the fluid volume and the sample volume, respectively, cm^3; and S is the integral area of the spectrum, which can be calculated by:

$$S = \int A(T_i)\, dT \quad (5)$$

where *A* is the spectrum amplitude at T_i.

The ϕ_P and ϕ_I can be determined by comparing the T_2 spectrum at S_w with that at S_{ir} for the same sample:[38]

$$\phi_P = \frac{FFI}{BFI + FFI} \times \phi_T;\ \phi_I = \frac{BFI}{BFI + FFI} \times \phi_T \quad (6)$$

where FFI and BFI are defined as the free and bound fluid index, respectively. To obtain these values, T_2 distribution measurements at S_w and S_{ir} were performed. Then the incremental T_2 spectra were transformed into accumulative ones, as shown in Figure 5. The accumulative amplitudes at S_w and S_{ir} are formatted to be equal to *BFI*+*FFI* and *BFI*, respectively.[38]

According to Eq. (6), the porosity of different pore types can be expressed as:

$$\phi_{Pi} = \frac{S_i}{S} \times \phi_P;\ \phi_{Ii} = \frac{S_i}{S} \times \phi_I \quad (7)$$

where i= 1,2,3 refer to macropores, mesopores, and micropores, and S_i denotes the integral area of the spectrum corresponding to different pore types, which can be expressed as:

$$S_1 = \int_0^{10} A(T_i)\, dT;\ S_2 = \int_{10}^{100} A(T_i)\, dT;\ S_3 = \int_{100}^{10000} A(T_i)\, dT \quad (8)$$

where S_1, S_2, and S_3 are the integral area of the spectrum of macropores, mesopores, and micropores, respectively.

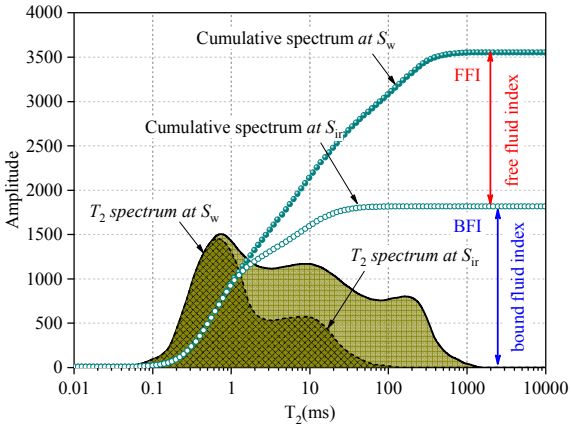

Figure 5. NMR measurements at S_w and S_{ir} showing the method to calculate *FFI* and *BFI*.[38, 44]

Permeability is the ability of coal to transport fluid and thus is a key property in evaluating reservoir productivity. Although coal permeability cannot be directly measured by NMR, it can be estimated based on the pore size distribution and connectivity through T_2 spectrum.[48] Currently, three models are widely accepted for NMR-determined permeability calculation: the *PP* model, the Coates model, and the SDR model.[49] Neither the PP model nor the Coates model is accurate for low permeable reservoir like coal.[50] Thus, the SDR model is applied in this paper:

$$k_N = 0.0224 \times \left(T_{2g}^a\right)^{1.534} \times \left(T_{2g}^b\right)^{0.182} \quad (9)$$

where k_N is the NMR-determined permeability, mD; T_{2g}^a and T_{2g}^b are the T_2 geometric means at S_w and S_{ir}, respectively, which can be calculated by:

$$T_{2g} = exp\left(\sum_{T_{2s}}^{T_{2max}} \frac{A_i}{A_T} ln(T_{2i})\right) \quad (4)$$

where T_{2s} is the transversal relaxation time at which the spectrum begins; T_{2i} is the individual value of T_2; T_{2max} is the maximum value of T_2; A_i is the amplitude at T_{2i}; and A_T is the total amplitude of the spectrum.

3.5. X-ray Computed Tomography.

An industrial X-ray computed tomography scanner (Diondo d5 manufactured by ND Inspection & Control Solution) was used to detect the internal fractures of coal (see Figure 3b). Image preparation and analysis were performed with the Avizo and the Image Processing Toolkit softwares.[51] After passing through the sample, the of X-ray signal can be attenuated by scattering and absorption. The attenuation (represented by the CT number) is proportional to the atomic number or the density of the sample.[52] Fractures, minerals, and the organic matter in coal samples can be distinguished by CT numbers due to the

density difference.[53-55] In addition, the fracture features (i.e. aperture, surface area, and volume) can be obtained by the Avizo software.

3.6. Acoustic Measurements.

Acoustic measurement is a useful method to describe rock structure and texture.[56] The measurements were conducted outside the microwave cavity using a HS-YS4 ultrasonic analyzer (see Figure 3c), which consists of a pulse generator, piezo-electric transducers, a signal conditioner, and a computer. The transducers (transmitter and receiver) were coupled to the coal sample via Vaseline. Signals from the pulse generator was transmitted to the sample at one end via the transmitter, picked up by the receiver attached to another end of the sample, then digitized and saved on the computer for processing. The P-wave velocity can be determined by eq (11).[57]

$$V_P = \frac{L}{\Delta t} \tag{11}$$

where V_P is the P-wave velocity, L is the length of the sample, and Δt is the transit time of the pulse.

4. RESULTS AND ANALYSIS

4.1. Evolution of Petrophysical Properties of the Centrifuged Coals.

It is commonly accepted that water exists in coal can be divided into free water and bound water.[58] The centrifuging experiment expels the free water within connective pores based on the Washburn equation:[50]

$$r_c = \frac{0.14}{P_c} \tag{12}$$

where P_c is the centrifuging pressure, MPa; and r_c is the minimum pore radius for water to discharge at the pressure P_c, μm.

According to eq (12), the centrifuging pressure of 1.4 MPa used in our experiments corresponds to a pore radius of 0.1 μm. This means that the water in the centrifuged coal including not only the bound water but also the free water left in the connective pores<0.1 μm.

The coal reservoir has multifaceted and hierarchical characteristics influenced by heterogeneity of the coal structures (Figure 6). That is, the coal is a network of pore and fracture systems.[59] The syngenetic fractures are termed cleat and classified into face cleat, butt cleat, master cleat, primary cleat, secondary cleat, and tertiary cleat (i.e. micro-fracture). Pores can be classified into micropores, mesopores, and macropores according to IUPAC.[60]

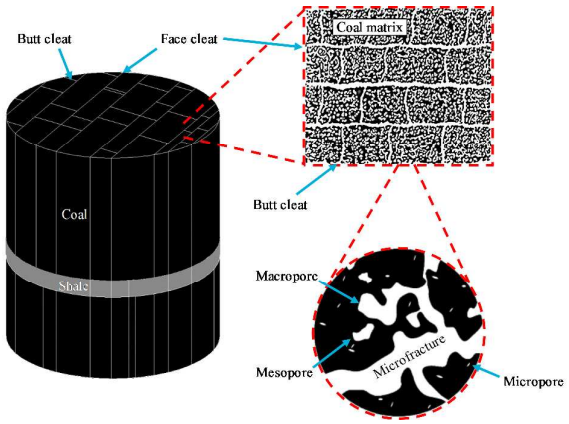

Figure 6. Pore and fracture systems of coal (modified from Flores[61]).

4.1.1. NMR T_2 Distribution.

The T_2 characteristics include the number, position, and size of T_2 spectrum peaks, which can be used to analyze coal pore distribution. Figure 7 illustrates the variations in T_2 spectra of the centrifuged coals with different microwave powers for S_{ir} and S_w cases. The T_2 spectrum of the raw coal consists of three separated peaks (i.e. P_1, P_2, and P_3), indicating large number of micropores and mesopores and small number of macropores. Compared to the T_2 spectrum at S_w, P_1 at S_{ir} remains unchanged, P_2 at S_{ir} lowers, and P_3 at S_{ir} disappears. This is a strong indication that micropores are always closed, while some mesopores as well as all macropores are inter-connected. The free fluids mainly migrate in macropores.

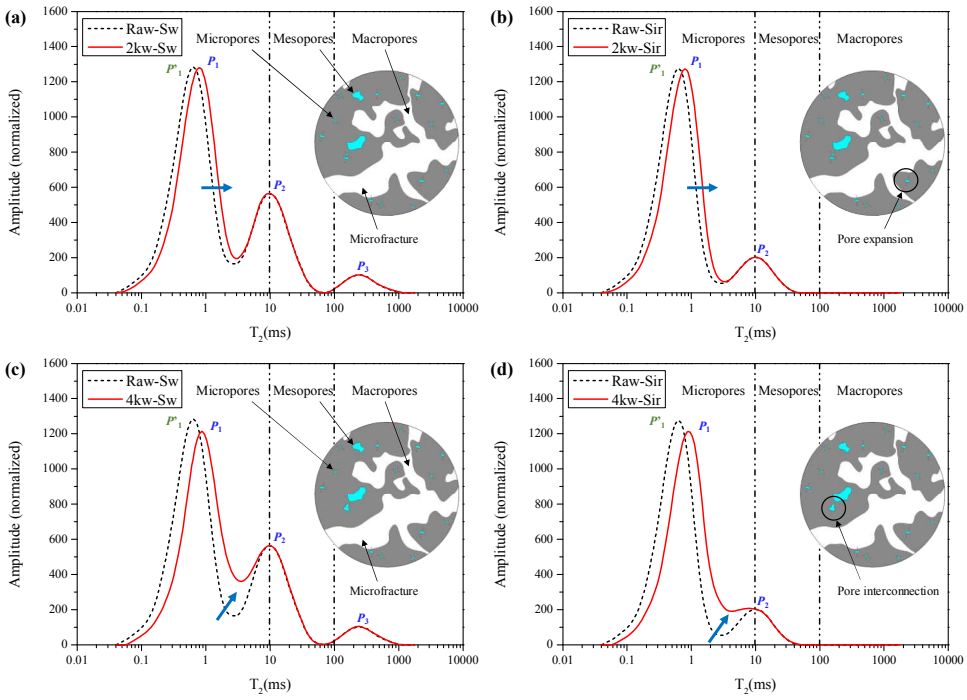

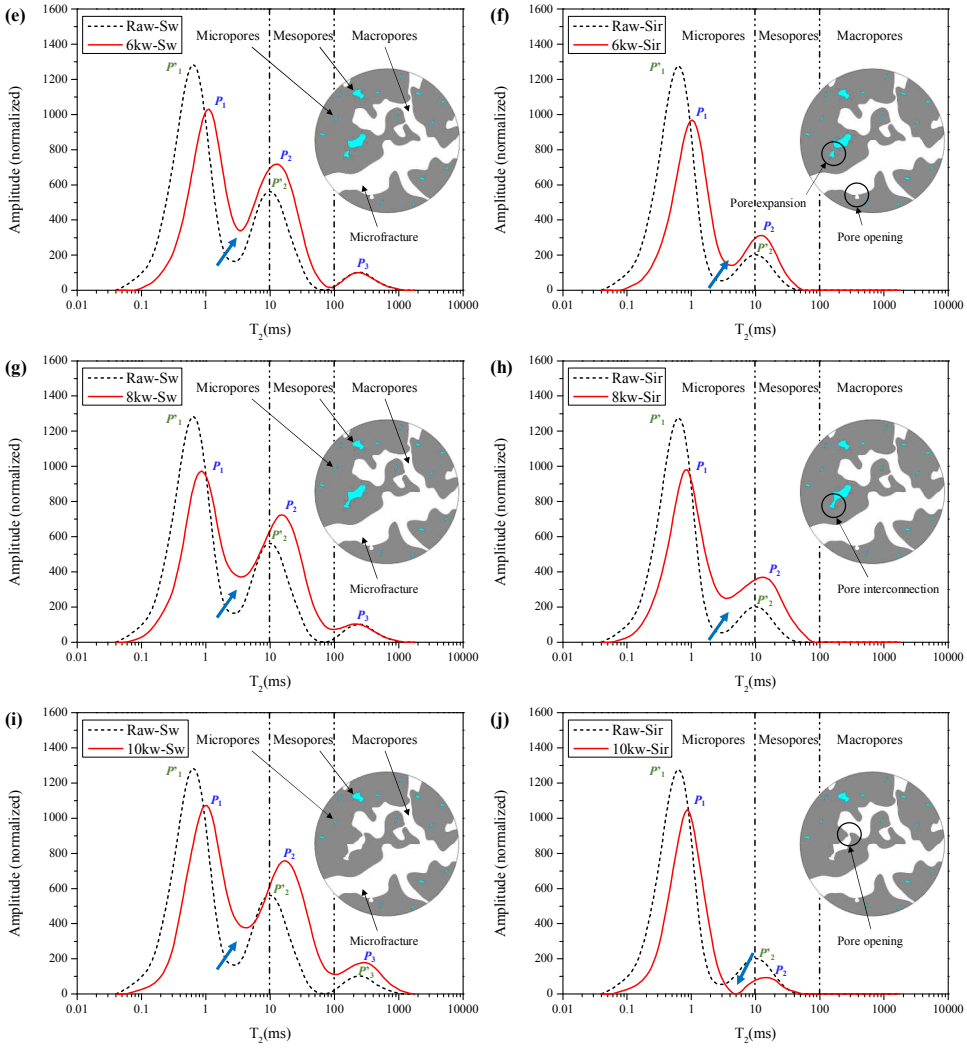

Figure 7. Variations in T_2 spectra of the centrifuged coals with different microwave powers.

After the coal has been microwave irradiated at 2 kW for 30 s, the location of P_1 at S_w and S_{ir} moves towards a longer transverse relaxation time corresponding to a larger pore size, which implies that microwave irradiation enlarges the micropores. When the microwave power increases to 4 kW, P_1 moves to the lower right, and the amplitude between P_1 and P_2 increases. This indicates that adjacent micropores are interconnected and integrated together to form larger pores. As the microwave power continually increases, P_1 lowers significantly, while P_2 and P_3 raise successively. This suggests that micropores are opened, and larger pores are formed. As discussed, all pores can be measured from a 100% saturated T_2 spectrum, but only closed pores and connective pores <0.1 μm can be measured from an irreducible water-saturated T_2 spectrum. When the microwave power reaches 10 kW, the T_2 spectrum of the irradiated coal at S_{ir} decreases significantly, while that at S_w still increases. This could be attributed to the fact that a considerable number of closed pores are opened and connected to the microfractures.

When the coal sample was irradiated under low microwave powers, the introduced water in the blind

or closed pores were first heated and then detached. On the one hand, the micropores collapsed because of the shrinkage forces caused by the moisture removal. On the other hand, the moisture was evaporated and expelled and, as a result, the jet flow pressure would open and link the pore structures.[36] Furthermore, the minerals such as pyrite in coal can be selectively heated and oxidized into pyrrhotite, which could be removed by the super-heated steam.[29] As the power increases, the moisture evaporation and mineral removal accelerate, resulting in intensive pore enlargement, opening, and interconnection.

4.1.2. Porosity, Permeability and P-wave Velocity.

Variations in the total porosity, irreducible porosity, and producible porosity with progressive microwave irradiation are illustrated in Figure 8. When the microwave power is lower than 6 kW, the porosity remains constant even though both the pore size and the pore number increase. With a further increase in the power, the total and producible porosity begin to show increasing trends, while the irreducible porosity has a decreasing trend. The producible porosity exceeds the irreducible porosity at 10 kW although it is initial lower. These reveal that microwave irradiation can facilitate the opening and connection of pores, which permits the coal reservoir to flow fluids to the drainage boreholes. As the microwave power increases, the porosity of micropores (especially the closed pores) reduces, while that of mesopores and macropores (especially the connective pores) increases.

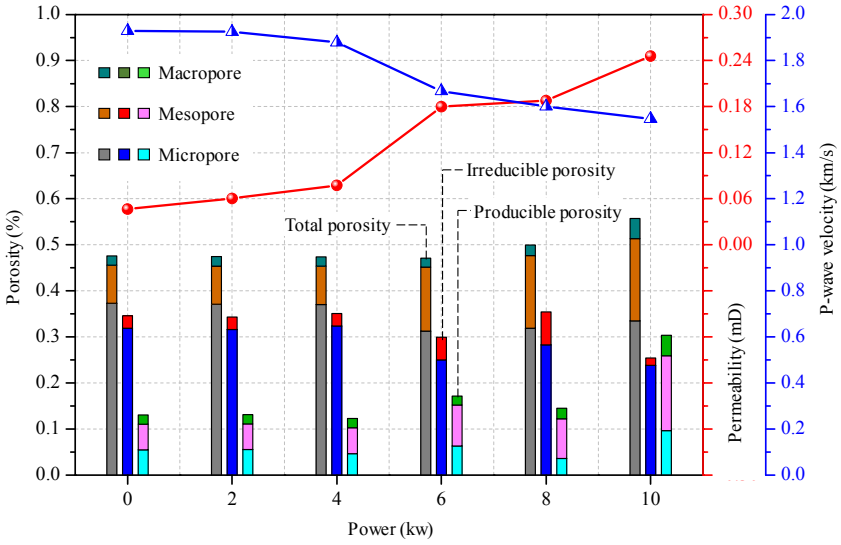

Figure 8. Variations in the porosity, permeability, and P-wave velocity of the centrifuged coals with microwave irradiation.

Figure 8 reveals that the determined porosity and permeability have increased by about 17 and 428% following the increase of the microwave power. Wang et al.[62] reported that the presence of water can reduce the coal permeability by up to two orders of magnitude. Microwave irradiation can also be regarded

as a dewatering process, which contributes to coal permeability enhancement.

It has been reported that the acoustic wave of a coal is closely related to the existence of pores and fractures.[56, 63] The existence of fractures would increase the energy attenuation of the acoustic wave and hence reduce the P-wave velocity.[64] In addition, the P-wave velocity has a decreasing trend with increasing angle between P-wave and fracture.[62] These could provide reference for the further study of fracture predicting.

Surface fracture sketches obtained from digital camera and the corresponding P-wave velocities monitored through the ultrasonic analyzer are shown in Figure 9. When the microwave power is lower than 4 kW, no fractures can be observed across the coal surface. As the microwave power reaches 4 kW, the P-wave velocity decreases from 1.93 km/s to 1.88 km/s because a fracture is generated from the top of the coal sample, propagating almost perpendicular to the face cleats. With a further increase in the power, the existing fractures in the coal cores start to propagate along the weak-lithotype banding, and new fractures gradually grow parallel to the face cleats, and thus the P-wave velocity decreases significantly.

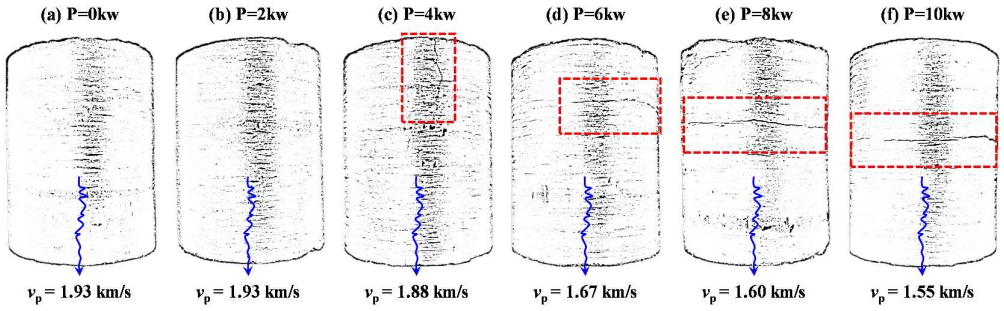

Figure 9. Evolutions of the surface fracture system and the corresponding P-wave velocities of the centrifuged coals with microwave irradiation.

4.2. Evolution of Petrophysical Properties of the Water-saturated Coals.

4.2.1. NMR T_2 Distribution.

Figure 10 shows variations in T_2 spectra at S_w of the centrifuged and water-saturated coals with microwave irradiation (black lines indicate the raw coals while colored lines indicate the irradiated coals). The microwave power produces the same effect on the centrifuged and water-saturated coals. As the microwave power increases, the locations of the T_2 peaks move towards longer transverse relaxation time corresponding to larger pore sizes, meaning that the pores are enlarged. In addition, the amplitude of P_1 decreases while those of P_2 and P_3 increase, demonstrating that the pores are integrated. Furthermore, the trough between peaks is generally enlarged, indicating that the pores are interconnected. When the microwave power keeps constant, the spectra amplitudes increase with increasing water contents.

Take P= 2 kW case for instance, when the water content is 1% (Figure 10b), the T_2 spectrum remains almost unchanged. This could be attributed to the water existing only or primarily in super-macropores or microfractures, having not penetrated into the macropores or smaller pores that can be shown in this T_2 spectrum distribution. Therefore, the irradiated water has little or no effect on the pore modification. Inevitably, surface or sub-surface pores could be occupied by water, which leads to the slight increase in the pore number under microwave irradiation of higher powers (P≥4 kW). When the water content reaches 3% (Figure 10c), the water almost fills the fractures and penetrate deeper into the internal macropores. The microwave irradiates the water in macropores, resulting in pore enlargement and the corresponding increase in P_3. The macropore enlargement continues until a water content of 6% is reached (Figure 10d). With further water penetration into mesopores, the pore size and number start to increase. The amplitude of P_2 exceeds that of P_1 after the microwave power has reached 6 kW, which means that the mesopores predominate. When the water content reaches 10% (Figure 10e), the amplitudes of peaks increase except P_3. This could be due to the fact that the macropores have been saturated with water while the micropores and mesopores are incompletely occupied. When the water content reaches 15% (Figure 10f), P_1 still enlarges while P_2 and P_3 cease to enlarge, indicating that all the mesopores and macropores have been completely saturated. Additionally, the isolated peaks of P_2 and P_3 gradually merge together and, as a result, the skewed trimodal T_2 distributions have been transformed into bimodal ones, demonstrating an improvement in the pore connectivity.

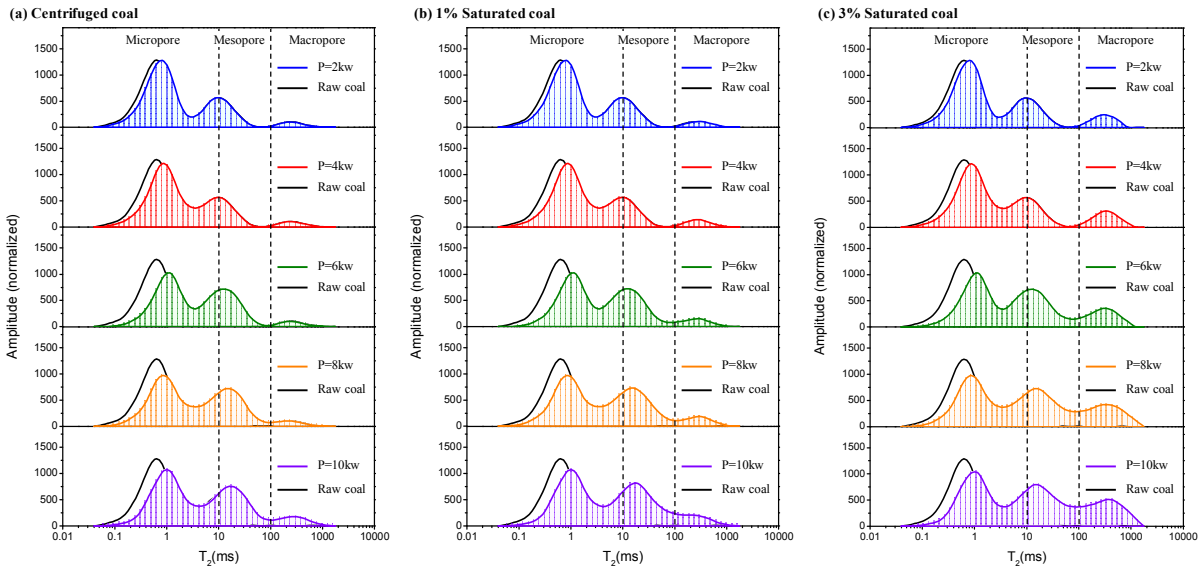

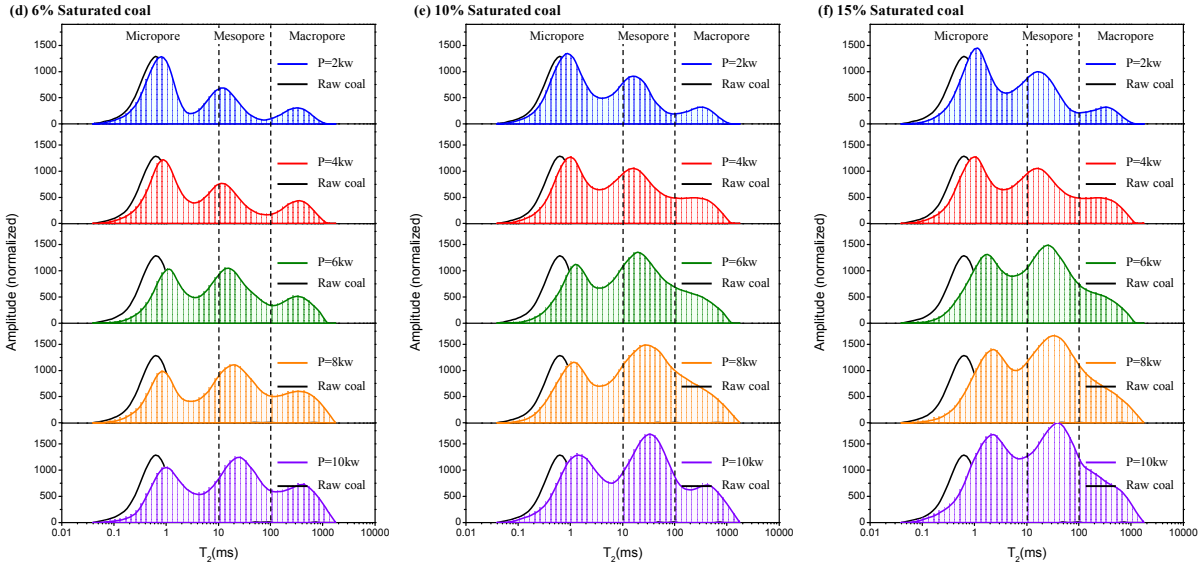

Figure 10. Variations in T_2 spectra of the water-saturated coals with microwave irradiation.

4.2.2. Porosity, Permeability and P-wave Velocity.

Mineral removal, moisture evaporation, and macromolecular decomposition caused by microwave irradiation have profound impact on the pore structure and thus affect the coal porosity.[32] Figure 11 illustrates variations in the total porosity and producible porosity of the water-saturated coals with progressive microwave irradiation. The two kinds of porosity show the same trend because the bound water in the samples occupies a small proportion. The total porosity and producible porosity of the raw coal are 0.48% and 0.13%, respectively, increasing linearly with the microwave power while grows exponentially with respect to the water content. When the water content increases from 0% to 3%, the porosity increases steadily by approximately 17~46% from its original value. The variation trend of porosity is different with respect to the pore size. Both the mesopores and macropores increase while the micropores decrease. When the water content is above 6%, the porosity increases rapidly by about 98~211% from its original value. The micropores increase at a flatter rate, while the mesopores and macropores show accelerating growth, and the porosity of the mesopores has the largest increment. This is a strong indication that the increase in the water content in the coal to be irradiated affects the pore distribution by enlarging the proportion of mesopores and macropores and pore interconnection.

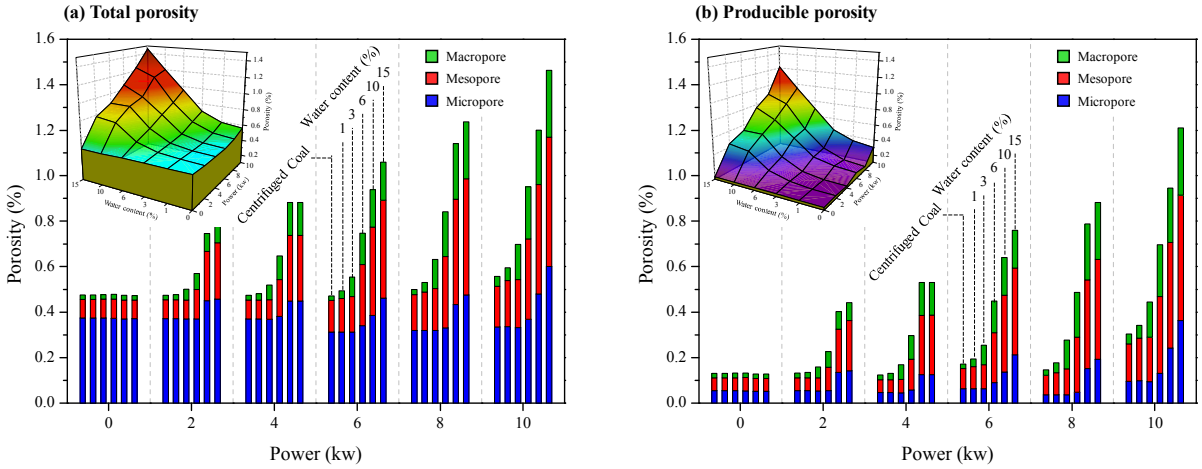

Figure 11. Variations in the porosity of the water-saturated coals with microwave irradiation.

Variations in the permeability and the P-wave velocity of the water-saturated coals with microwave irradiation are depicted in Figures. 12a and b, respectively. In general, as the water content increases, the permeability increases while the corresponding P-wave velocity decreases. When the water content is lower than 1% and the microwave power is lower than 4 kW, the permeability and the P-wave velocity remain unchanged because limited pores and fractures have been generated by microwave irradiation. Further increase in the microwave power starts to enlarge the permeability and reduce the P-wave velocity. For the cases of water contents ranging from 3 to 6% by mass, the permeability and the P-wave velocity vary significantly at accelerating rates. This could be attributed to the enlargement, interconnection, and integration of pores and the generation of fractures induced by microwave irradiation. When the water content is 6% and the microwave power reaches 10 kW, the P-wave velocity decreases to zero because the growing fractures cut off the propagation of the acoustic wave. Here, the microwave power at which the P-wave velocity disappears is defined as the cut off power. This power indicates the capacity of microwave fracturing. It can be seen from Figure 12 that the cut off power decreases with the water content (6~15%), indicating that the water content dominates microwave fracturing and reduces energy consumption. When the water content ranges from 10 to 15%, the permeability increases, showing a peak at 8 kW followed by a decline, which suggests the optimum power of 8 kW for coal fracturing. This phenomenon will be explained in the next section.

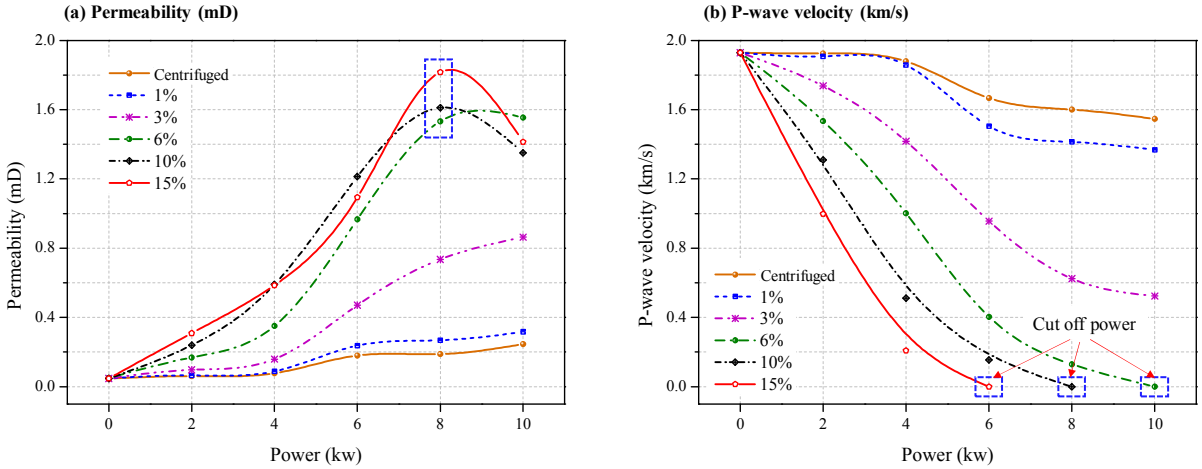

Figure 12. Variations in the permeability and the P-wave velocity of the water-saturated coals with microwave irradiation.

4.2.3. Fracture Distribution.

An industrial X-ray computed tomography (CT) scanner was applied to quantitatively evaluate variations in the fracture distribution and visualization of coals with microwave irradiation. The scatter diagram of fracture distribution of the raw coal is presented in Figure 13a, where the x, y coordinates refer to the fracture volume and fracture number, respectively. Here, an opening extending along a plane with aperture difference smaller than 20% is regarded as a single fracture. Obviously, the fracture distribution is skewed trumpet-shaped, indicating that the major fractures are composed of branch microfractures, which are predominant in the raw coal. For better analysis, the number statistics of fractures with respect to the fracture volume was conducted, as illustrated in Figure 13b (e.g. the point at 0.02 mm^3 represents the number of fractures range from 0.01 mm^3 to 0.02 mm^3). As the fracture volume increases, the fracture number generally decreases, and three peak values (i.e. P_1, P_2, and P_3) appear at 0.004 mm^3, 0.02 mm^3, and 0.2 mm^3. The 3D reconstruction of the coal generated from the X-ray CT consists of gray scale pixels, as shown in Figure 13c. Minerals have a higher density than the coal matrix and thus appear as bright white particles. On the contrary, the natural fractures with different apertures appear as colored lines because of the low density. It can be seen that most fractures in the raw coal are mineral occluded, heterogeneously distributed with poor connectivity. Mineral occlusions have the potential to block fluid-flow pathways, reducing coal permeability.

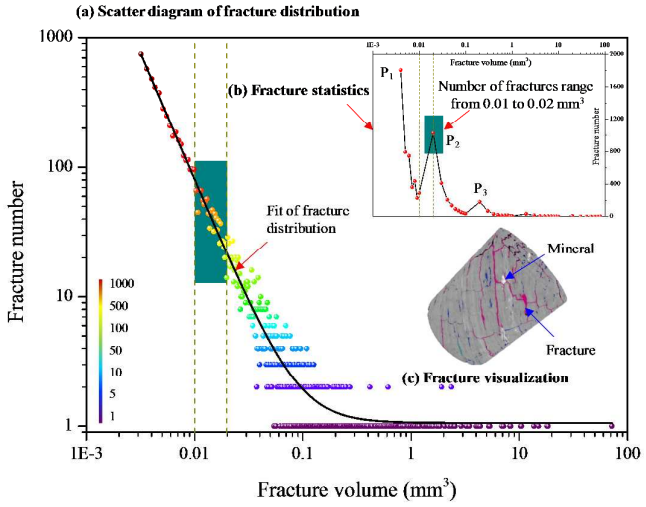

Figure 13. Fracture distribution and visualization of the raw coal.

Figure 14 shows the progressive changes in the fracture statistics of the centrifuged and water-saturated coals with microwave irradiation. For the centrifuged coal (Figure 14a), the bound water is predominant while the free water is limited. On the one hand, the interaction of the bound water with the microwaves has significant effect on the pore structure, but it exerts little effect on the fracture system. As a result, the global fracture distribution is slightly affected. On the other hand, the mineral particles bounded in the microfractures are first heated and then detached under microwave irradiation. As a result, the mineral-occluded fractures which volume ranges from 0.004 to 0.006 mm^3 are dredged, extended, and increased in volume with increasing microwave power. When the water content is 1% (Figure 14b), mineral erosion continues within 0.004~0.006 mm^3, and a new peak (P_4) emerges between 1 and 10 mm^3. At this stage, the water has penetrated into the major factures which volume is greater than 1 mm^3. The interaction of the free water with the microwave enlarges the aperture, length, and volume of the fractures. With further penetration of water (3%), P_4 increases and develops towards larger volumes. This indicates that larger factures with volume greater than 10 mm^3 have been created. With additional water penetration (6%), P_3 increases sharply while P_4 increases slightly. The fractures continue to widen and propagate deeper into the coal to connect to each other. At this stage, a fracture network has been generated throughout the coal core. As the water content proceed to increase (10 and 15%), the effect of microwave irradiation on the water becomes more and more significantly. As a result, P_2 (0.004 mm^3) and P_1 (0.02 mm^3) grow successively. Well-connected and non-mineralized fractures with larger volume distribution ranges have been generated.

The differential heating of microwaves creates a thermal gradient between the host matrix and the heated phase, which in turn induces inhomogeneous thermal expansion, thermal stresses, and fractures.[36]

As the microwave power increases, the thermal gradient enlarges. Therefore, more fractures with larger apertures and lengths would be formed. However, once the power reaches 8 kW and the water content reaches 6%, the heat conduction is enhanced to equalize the thermal field within the coal, which can be used to explain the permeability reduction as shown in Figure 12a. These findings are in good agreement with those reported by Kumar et al.[40] It has been stated that the dielectric property of coal increases with increasing water content.[65, 66] At the same microwave power, higher water content strengthens differential heating and, as a result, creates more fractures.

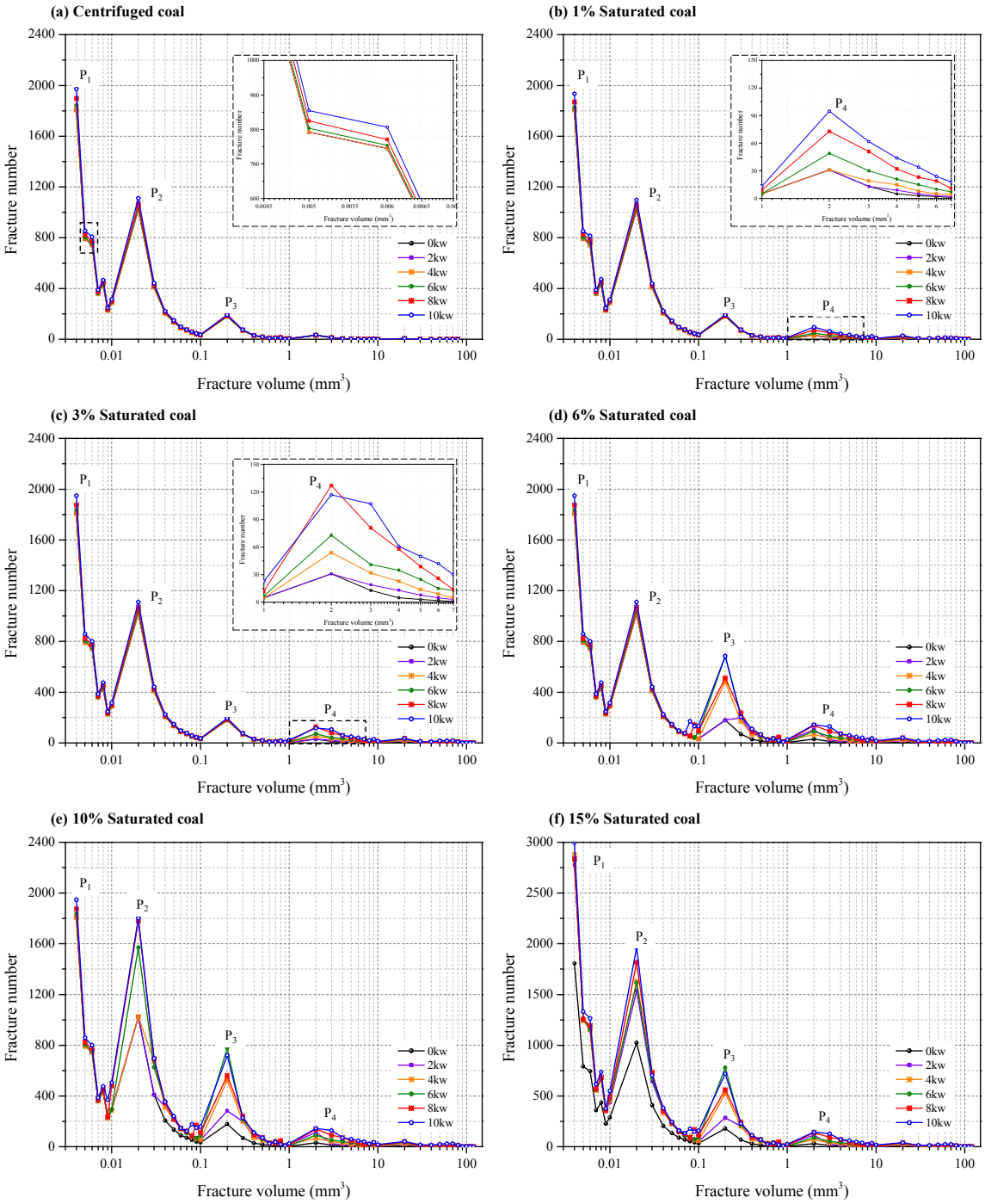

Figure 14. Variations in the fracture distribution of the centrifuged and water-saturated coals with microwave irradiation.

5. POTENTIAL APPLICATION

Microwave heating has been studied for many years in the petroleum industry.[67] The main purpose in the practice is to heat the reservoir by an antenna or an induction coil inserted into the injector. As the reservoir temperature increases, oil viscosity reduces and starts to flow towards the production well.[68] In 1986, microwave heating was first implemented in the Wildmere Field, Alberta to increase the heavy oil production.[69] After applying microwave heating, the production rate was increased from 0.95 tonnes/day to 3.18 tonnes/day. Borrowing from these studies, we can conclude that microwave irradiation through antennae can be a suitable method for coal bed degassing.

As shown in Figure 15, the system consists of:

- a CBM well, which is designed to host microwave apparatus and a CBM extraction tube;
- microwave apparatus including a microwave generator, a waveguide to coax transition, rectangular and coaxial waveguides, and an antenna, and
- a Teflon tube, which is a microwave-transparent structure interposed to safeguard the well.

Once combined with hydraulic technologies such as hydro-fracturing, -flushing, and -slotting, microwave can heat the residual water in the fractures. On the one hand, gas migration channels (i.e. pores and fractures) will be enlarged, opened, and interconnected. On the other hand, methane desorption can be enhanced due to the effects of warming and dewatering caused by microwave irradiation. As a result, the CBM production will be greatly enhanced.

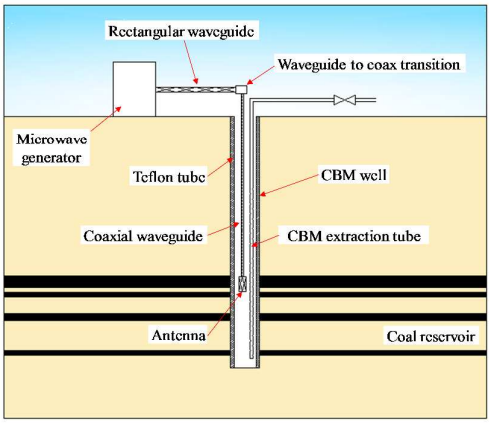

Figure 15. Conceptual design of a CBM production well with microwave irradiation.[38, 70]

6. CONCLUSIONS

This paper evaluated the evolution of coal petrophysical properties under microwave irradiation stimulation with different water contents ranging from 1 to 15%. A series of experiments were conducted on a bituminous coal through a suite of integrated diagnostic techniques including Nuclear Magnetic Resonance (NMR) and X-ray Computed Tomography (X-CT).

The mineral removal and moisture evaporation due to the microwave selective heating lead to pore enlargement, opening, and interconnection. The total porosity increases linearly with the microwave power while grows exponentially with respect to water contents. The increase in the water content affects the pore distribution by enlarging the proportion of mesopores and macropores and pore connectivity. The differential heating of microwaves creates a thermal gradient, which in turn induces inhomogeneous thermal expansion, thermal stresses, and fractures. The microwave power creates fractures by enlarging the thermal gradient, and the water content affect fractures by increasing the dielectric property. As a result, the permeability increases, while the P-wave velocity decreases.

The significant enhancement of coal permeability and pore fracture structure indicates that the microwave irradiation is effective in improving gas productivity thus has the potential to become a new CBM reservoir simulation technology.

■ AUTHOR INFORMATION

Corresponding Author

*Tel: +86 051683884401. E-mail address: lbq21405@126.com (B. Lin).

Notes

The authors declare no competing financial interest.

■ ACKNOWLEDGEMENTS

This work was supported by the Fundamental Research Funds for the Central Universities (2017BSCXB06).

■ REFERENCES

(1) Moore, T.A. Coalbed methane: A review. *Int. J. Coal Geol.* **2012**, 101, 36-81.

(2) Tang, S.; Wan, Y.; Duan, L.; Xia, Z.; Zhang, S. Methane adsorption-induced coal swelling measured with an optical method. *Int. J. Min. Sci. Technol.* **2015**, 25(6), 949-953.

(3) Skoczylas, N. Laboratory study of the phenomenon of methane and coal outburst. *Int. J. Rock Mech. Min. Sci.* **2012**, 55, 102-107.

(4) Szlązak, N.; Obracaj, D.; Swolkień, J. Methane drainage from roof strata using an overlying drainage

gallery. *Int. J. Coal Geol.* **2014**, 136, 99-115.

(5) Zhou, L.; Pritchard, C.; Zheng, Y. CFD modeling of methane distribution at a continuous miner face with various curtain setback distances. *Int. J. Min. Sci. Technol.* **2015**, 25(4), 635-640.

(6) Li, H.; Lin, B.; Yang, W.; Gao, Y.; Liu, T. Effects of an underlying drainage gallery on coal bed methane capture effectiveness and the mechanical behavior of a gate road. *J. Nat. Gas Sci. Eng.* **2015**, 27, 616-631.

(7) Karacan, C.Ö.; Ruiz, F.A.; Cotè, M.; Phipps, S. Coal mine methane: A review of capture and utilization practices with benefits to mining safety and to greenhouse gas reduction. *Int. J. Coal Geol.* **2011**, 86(2-3), 121-156.

(8) Qin, L.; Zhai, C.; Liu, S.; Xu, J.; Tang, Z.; Yu, G. Failure Mechanism of Coal after Cryogenic Freezing with Cyclic Liquid Nitrogen and Its Influences on Coalbed Methane Exploitation. *Energy Fuels* **2016**, 30(10), 8567-8578.

(9) White, C.M.; Smith, D.H.; Jones, K.L.; Goodman, A.L.; Jikich, S.A.; LaCount, R.B.; DuBose, S.B.; Ozdemir, E.; Morsi, B.I.; Schroeder, K.T. Sequestration of carbon dioxide in coal with enhanced coalbed methane recovery - A review. *Energy Fuels* **2005**, 19(3), 659-724.

(10) Guo, J.; Kang, T.; Kang, J.; Chai, Z.; Zhao, G. Accelerating methane desorption in lump anthracite modified by electrochemical treatment. *Int. J. Coal Geol.* **2014**, 131, 392-399.

(11) Zheng, C.; Chen, Z.; Kizil, M.; Aminossadati, S.; Zou, Q.; Gao, P. Characterisation of mechanics and flow fields around in-seam methane gas drainage borehole for preventing ventilation air leakage: A case study. *Int. J. Coal Geol.* **2016**, 162, 123-138.

(12) Mohd Yasin, N.H.; Maeda, T.; Hu, A.; Yu, C.-P.; Wood, T.K. CO2 sequestration by methanogens in activated sludge for methane production. *Appl. Energy* **2015**, 142, 426-434.

(13) Cai, C.; Li, G.; Huang, Z.; Tian, S.; Shen, Z.; Fu, X. Experiment of coal damage due to super-cooling with liquid nitrogen. *J. Nat. Gas Sci. Eng.* **2015**, 22, 42-48.

(14) Huang, B.; Cheng, Q.; Chen, S. Phenomenon of methane driven caused by hydraulic fracturing in methane-bearing coal seams. *Int. J. Min. Sci. Technol.* **2016**, 26(5), 919-927.

(15) Huang, W.A.; Lei, M.; Qiu, Z.S.; Leong, Y.K.; Zhong, H.Y.; Zhang, S.F. Damage mechanism and protection measures of a coalbed methane reservoir in the Zhengzhuang block. *J. Nat. Gas Sci. Eng.* **2015**, 26, 683-694.

(16) Bahrami, H.; Rezaee, R.; Clennell, B. Water blocking damage in hydraulically fractured tight sand gas reservoirs: An example from Perth Basin, Western Australia. *J Petrol Sci Eng* **2012**, 88-89, 100-106.

(17) Ni, G.; Cheng, W.; Lin, B.; Zhai, C. Experimental study on removing water blocking effect (WBE) from two aspects of the pore negative pressure and surfactants. *J. Nat. Gas Sci. Eng.* **2016**, 31, 596-602.

(18) Liu, H.; Xu, L.; Jin, Y.; Fan, B.; Qiao, X.; Yang, Y. Effect of coal rank on structure and dielectric properties of chars. *Fuel* **2015**, 153, 249-256.

(19) Martinez-Guerra, E.; Gude, V.G.; Mondala, A.; Holmes, W.; Hernandez, R. Microwave and ultrasound enhanced extractive-transesterification of algal lipids. *Appl. Energy* **2014**, 129, 354-363.

(20) Jerby, E.; Dikhtyar, V.; Aktushev, O.; Grosglick, U. The microwave drill. *Science* **2002**, 298(5593), 587-9.

(21) Maskan, M. Microwave/air and microwave finish drying of banana. *J. Food Eng.* **2000**, 44(2), 71-78.

(22) Binner, E.; Lester, E.; Kingman, S.; Dodds, C.; Robinson, J.; Wu, T.; Wardle, P.; Mathews, J.P. A Review of Microwave Coal Processing. *Journal of Microwave Power and Electromagnetic Energy* **2014**, 48(1), 35-60.

(23) Marland, S.; Han, B.; Merchant, A.; Rowson, N. The effect of microwave radiation on coal grindability. *Fuel* **2000**, 79(11), 1283-1288.

(24) Tahmasebi, A.; Yu, J.; Li, X.; Meesri, C. Experimental study on microwave drying of Chinese and Indonesian low-rank coals. *Fuel Process. Technol.* **2011**, 92(10), 1821-1829.

(25) Lester, E.; Kingman, S.; Dodds, C. Increased coal grindability as a result of microwave pretreatment at economic energy inputs. *Fuel* **2005**, 84(4), 423-427.

(26) Uslu, T.; Atalay, Ü. Microwave heating of coal for enhanced magnetic removal of pyrite. *Fuel Process. Technol.* **2004**, 85(1), 21-29.

(27) Lester, E.; Kingman, S.; Dodds, C.; Patrick, J. The potential for rapid coke making using microwave energy. *Fuel* **2006**, 85(14-15), 2057-2063.

(28) Folorunso, O.; Dodds, C.; Dimitrakis, G.; Kingman, S. Continuous energy efficient exfoliation of vermiculite through microwave heating. *Int. J. Miner. Process.* **2012**, 114-117, 69-79.

(29) Wang, J.; Li, Y. Synergistic pretreatment of waste activated sludge using CaO_2 in combination with microwave irradiation to enhance methane production during anaerobic digestion. *Appl. Energy* **2016**, 183, 1123-1132.

(30) Lester, E.; Kingman, S. The effect of microwave pre-heating on five different coals. *Fuel* **2004**, 83(14-15), 1941-1947.

(31) Kingman, S.W. Recent developments in microwave processing of minerals. *Int. Mater. Rev.* **2013**, 51(1), 1-12.

(32) Seehra, M.S.; Kalra, A.; Manivannan, A. Dewatering of fine coal slurries by selective heating with microwaves. *Fuel* **2007**, 86(5-6), 829-834.

(33) Sahoo, B.K.; De, S.; Meikap, B.C. Improvement of grinding characteristics of Indian coal by microwave pre-treatment. *Fuel Process. Technol.* **2011**, 92(10), 1920-1928.

(34) Whittles, D.N.; Kingman, S.W.; Reddish, D.J. Application of numerical modelling for prediction of the influence of power density on microwave-assisted breakage. *Int. J. Miner. Process.* **2003**, 68(1-4), 71-91.

(35) Liu, J.-Z.; Zhu, J.-F.; Cheng, J.; Zhou, J.-H.; Cen, K.-F. Pore structure and fractal analysis of Ximeng lignite under microwave irradiation. *Fuel* **2015**, 146, 41-50.

(36) Kumar, H.; Lester, E.; Kingman, S.; Bourne, R.; Avila, C.; Jones, A.; Robinson, J.; Halleck, P.M.; Mathews, J.P. Inducing fractures and increasing cleat apertures in a bituminous coal under isotropic stress via application of microwave energy. *Int. J. Coal Geol.* **2011**, 88(1), 75-82.

(37) Ge, L.; Zhang, Y.; Wang, Z.; Zhou, J.; Cen, K. Effects of microwave irradiation treatment on physicochemical characteristics of Chinese low-rank coals. *Energy Conv. Manag.* **2013**, 71, 84-91.

(38) Li, H.; Lin, B.; Yang, W.; Zheng, C.; Hong, Y.; Gao, Y.; Liu, T.; Wu, S. Experimental study on the petrophysical variation of different rank coals with microwave treatment. *Int. J. Coal Geol.* **2016**, 154-155, 82-91.

(39) Tang, Z.; Zhai, C.; Zou, Q.; Qin, L. Changes to coal pores and fracture development by ultrasonic wave excitation using nuclear magnetic resonance. *Fuel* **2016**, 186, 571-578.

(40) Li, S.; Tang, D.; Pan, Z.; Xu, H.; Huang, W. Characterization of the stress sensitivity of pores for different rank coals by nuclear magnetic resonance. *Fuel* **2013**, 111, 746-754.

(41) Ohkubo, T.; Ibaraki, M.; Tachi, Y.; Iwadate, Y. Pore distribution of water-saturated compacted clay using NMR relaxometry and freezing temperature depression; effects of density and salt concentration. *Appl. Clay Sci.* **2016**, 123, 148-155.

(42) Lewis, R.T.; Seland, J.G. A multi-dimensional experiment for characterization of pore structure heterogeneity using NMR. *J. Magn. Reson.* **2016**, 263, 19-32.

(43) Ouyang, Z.; Liu, D.; Cai, Y.; Yao, Y. Fractal Analysis on Heterogeneity of Pore–Fractures in Middle–High Rank Coals with NMR. *Energy Fuels* **2016**, 30(7), 5449-5458.

(44) Zhai, C.; Qin, L.; Liu, S.; Xu, J.; Tang, Z.; Wu, S. Pore Structure in Coal: Pore Evolution after Cryogenic Freezing with Cyclic Liquid Nitrogen Injection and Its Implication on Coalbed Methane Extraction. *Energy Fuels* **2016**, 30(7), 6009-6020.

(45) Yao, Y.; Liu, D.; Xie, S. Quantitative characterization of methane adsorption on coal using a low-field NMR relaxation method. *Int. J. Coal Geol.* **2014**, 131, 32-40.

(46) Xu, H.; Tang, D.; Zhao, J.; Li, S. A precise measurement method for shale porosity with low-field nuclear magnetic resonance: A case study of the Carboniferous–Permian strata in the Linxing area, eastern Ordos Basin, China. *Fuel* **2015**, 143, 47-54.

(47) Li, S.; Tang, D.; Xu, H.; Yang, Z. Advanced characterization of physical properties of coals with different coal structures by nuclear magnetic resonance and X-ray computed tomography. *Comput. Geosci.* **2012**, 48, 220-227.

(48) Pan, Z.; Connell, L.D.; Camilleri, M. Laboratory characterisation of coal reservoir permeability for primary and enhanced coalbed methane recovery. *Int. J. Coal Geol.* **2010**, 82(3-4), 252-261.

(49) Cai, Y.; Liu, D.; Pan, Z.; Yao, Y.; Li, J.; Qiu, Y. Petrophysical characterization of Chinese coal cores with

heat treatment by nuclear magnetic resonance. *Fuel* **2013**, 108, 292-302.

(50) Yao, Y.; Liu, D.; Che, Y.; Tang, D.; Tang, S.; Huang, W. Petrophysical characterization of coals by low-field nuclear magnetic resonance (NMR). *Fuel* **2010**, 89(7), 1371-1380.

(51) Mathews, J.P.; Pone, J.D.N.; Mitchell, G.D.; Halleck, P. High-resolution X-ray computed tomography observations of the thermal drying of lump-sized subbituminous coal. *Fuel Process. Technol.* **2011**, 92(1), 58-64.

(52) Pone, J.D.N.; Halleck, P.M.; Mathews, J.P. 3D characterization of coal strains induced by compression, carbon dioxide sorption, and desorption at in-situ stress conditions. *Int. J. Coal Geol.* **2010**, 82(3-4), 262-268.

(53) Mazumder, S.; Wolf, K.H.A.A.; Elewaut, K.; Ephraim, R. Application of X-ray computed tomography for analyzing cleat spacing and cleat aperture in coal samples. *Int. J. Coal Geol.* **2006**, 68(3-4), 205-222.

(54) Heriawan, M.N.; Koike, K. Coal quality related to microfractures identified by CT image analysis. *Int. J. Coal Geol.* **2015**, 140, 97-110.

(55) Golab, A.; Ward, C.R.; Permana, A.; Lennox, P.; Botha, P. High-resolution three-dimensional imaging of coal using microfocus X-ray computed tomography, with special reference to modes of mineral occurrence. *Int. J. Coal Geol.* **2013**, 113, 97-108.

(56) Khandelwal, M.; Singh, T.N. Correlating static properties of coal measures rocks with P-wave velocity. *Int. J. Coal Geol.* **2009**, 79(1-2), 55-60.

(57) Müller-Huber, E.; Schön, J.; Börner, F. Pore space characterization in carbonate rocks — Approach to combine nuclear magnetic resonance and elastic wave velocity measurements. *J. Appl. Geophys.* **2016**, 127, 68-81.

(58) Yu, J.; Tahmasebi, A.; Han, Y.; Yin, F.; Li, X. A review on water in low rank coals: The existence, interaction with coal structure and effects on coal utilization. *Fuel Process. Technol.* **2013**, 106, 9-20.

(59) Zolfaghari, A.; Piri, M. Pore-Scale Network Modeling of Three-Phase Flow Based on Thermodynamically Consistent Threshold Capillary Pressures. I. Cusp Formation and Collapse. *Transport in Porous Media* **2017**, 116(3), 1093-1137.

(60) Li, Z.W.; Lin, B.Q.; Gao, Y.B.; Cao, Z.D.; Cheng, Y.Y.; Yu, J.Y. Fractal analysis of pore characteristics and their impacts on methane adsorption of coals from Northern China. *Int J Oil Gas Coal T* **2015**, 10(3), 306-324.

(61) FLORES, R.M. *COAL AND COALBED GAS-FUELING THE FUTURE*; Elsevier: Waltham, MA 2014; pp 219-221.

(62) Cai, Y.; Liu, D.; Mathews, J.P.; Pan, Z.; Elsworth, D.; Yao, Y.; Li, J.; Guo, X. Permeability evolution in fractured coal — Combining triaxial confinement with X-ray computed tomography, acoustic emission and

ultrasonic techniques. *Int. J. Coal Geol.* **2014**, 122, 91-104.

(63) Song, I.; Suh, M. Effects of foliation and microcracks on ultrasonic anisotropy in retrograde ultramafic and metamorphic rocks at shallow depths. *J. Appl. Geophys.* **2014**, 109, 27-35.

(64) Wang, H.; Pan, J.; Wang, S.; Zhu, H. Relationship between macro-fracture density, P-wave velocity, and permeability of coal. *J. Appl. Geophys.* **2015**, 117, 111-117.

(65) Fan, W.; Jia, C.; Hu, W.; Yang, C.; Liu, L.; Zhang, X.; Chang, T.; Cui, H.-L. Dielectric properties of coals in the low-terahertz frequency region. *Fuel* **2015**, 162, 294-304.

(66) Wang, Q.; Zhang, X.; Gu, F. Investigation on interior moisture distribution inducing dielectric anisotropy of coals. *Fuel Process. Technol.* **2008**, 89(6), 633-641.

(67) Bera, A.; Babadagli, T. Status of electromagnetic heating for enhanced heavy oil/bitumen recovery and future prospects: A review. *Appl. Energy* **2015**, 151, 206-226.

(68) Kasevich, R.S. Method and apparatus for in-situ radiofrequency assisted gravity drainage of oil (RAGD). **2008**, US.

(69) Spencer, H.L. Electromagnetic Oil Recovery Ltd, Calgary, Canada. 1987.

(70) Hong, Y.-d.; Lin, B.-q.; Zhu, C.-j.; Li, H. Effect of microwave irradiation on petrophysical characterization of coals. *Appl. Therm. Eng.* **2016**, 102, 1109-1125.